AFRL-DE-PS-
TR-2005-1030

CONFORMAL IMPULSE RECEIVE ANTENNA ARRAYS

D. V. Giri, et al.

Pro-Tech
11-C Orchard Court
Alamo, CA 94507-1541

23 February 2005

Final Report

AIR FORCE RESEARCH LABORATORY
Directed Energy Directorate
3550 Aberdeen Ave SE
AIR FORCE MATERIEL COMMAND
KIRTLAND AIR FORCE BASE, NM 87117-5776

STINFO COPY

AFRL-DE-PS-TR-2005-1030

Using Government drawings, specifications, or other data included in this document for any purpose other than Government procurement does not in any way obligate the U.S. Government. The fact that the Government formulated or supplied the drawings, specifications, or other data, does not license the holder or any other person or corporation; or convey any rights or permission to manufacture, use, or sell any patented invention that may relate to them.

This report has been reviewed by the Public Affairs Office and is releasable to the National Technical Information Service (NTIS). At NTIS, it will be available to the general public, including foreign nationals.

If you change your address, wish to be removed from this mailing list, or your organization no longer employs the addressee, please notify AFRL/DEHP, 3550 Aberdeen Ave SE, Kirtland AFB, NM 87117-5776.

Do not return copies of this report unless contractual obligations or notice on a specific document requires its return.

This report has been approved for publication.

//SIGNED//
JOSEPH L. BROECKERT, 2d Lt, USAF
Project Manager

//SIGNED//
THOMAS A. SPENCER, DR-IV
Acting Chief, High Power Microwave Division
Directorate

//SIGNED//
L. BRUCE SIMPSON, SES
Director, Directed Energy

REPORT DOCUMENTATION PAGE

Form Approved
OMB No. 0704-0188

1. REPORT DATE *(DD-MM-YYYY)*	2. REPORT TYPE	3. DATES COVERED *(From - To)*
23-02-2005	Final Report	16 Apr 04–15 Apr 05

4. TITLE AND SUBTITLE
CONFORMAL IMPULSE RECEIVE ANTENNA ARRAYS

5a. CONTRACT NUMBER
FA9451-04-M-0081

5b. GRANT NUMBER
N/A

5c. PROGRAM ELEMENT NUMBER
65502F

6. AUTHOR(S)
D. V. Giri*, K. F. Casey*, M.C. Skipper and M.D. Abdalla

5d. PROJECT NUMBER
3005

5e. TASK NUMBER
DP

5f. WORK UNIT NUMBER
DJ

7. PERFORMING ORGANIZATION NAME(S) AND ADDRESS(ES)

*Pro-Tech
11-C Orchard Court
Alamo, CA 94507-1541

ASR Corporation
7817 Bursera Dr SW
Albuquerque, NM 87120

8. PERFORMING ORGANIZATION REPORT
Project 509-Final

9. SPONSORING / MONITORING AGENCY NAME(S) AND ADDRESS(ES)

Air Force Research Laboratory
3550 Aberdeen Avenue SE
Kirtland AFB, NM 87117-5776

10. SPONSOR/MONITOR'S ACRONYM(S)
AFRL/DEHP

11. SPONSOR/MONITOR'S REPORT NUMBER(S)
AFRL-DE-PS-TR-2005-1030

12. DISTRIBUTION / AVAILABILITY STATEMENT
APPROVED FOR PUBLIC RELEASE; DISTRIBUTION IS UNLIMITED.

13. SUPPLEMENTARY NOTES

14. ABSTRACT

This report addresses the design and fabrication of a prototype transient multi-element planar array operating in an impulse regime. The objective is to develop a conformal impulse "timed-array" antenna, operating in a transient regime and covering a wide frequency band spanning an approximately 200 MHz-2 GHz range. Under this Phase-I effort, we have analytically formulated the receiving characteristics of a hyperband antenna array. In addition, a mock-up four element conformal antenna was built and evaluated. The antenna utilizes a nylon substrate. The results indicate that the theoretical basis for the antenna is valid and that some simple improvements can be done to substantially improve the performance.

15. SUBJECT TERMS Conformal antennas, Bow-tie antennas, Antenna Arrays, UAV, Global Hawk, Composite materials, Radiation Patterns

16. SECURITY CLASSIFICATION OF:			17. LIMITATION OF	18. NUMBER OF	19a. NAME OF RESPONSIBLE PERSON
a. REPORT	b. ABSTRACT	c. THIS PAGE			Lt Joseph Broeckert
U	U	U	SAR	50	19b. TELEPHONE NUMBER *(include area code)* (505) 853-4707

Standard Form 298 (Rev. 8-98)
Prescribed by ANSI Std. Z39.18

(This page is intentionally left blank)

TABLE OF CONTENTS

LIST OF FIGURES

Conformal Impulse Receive Antenna Arrays

1. Background

Conformal arrays are of great importance in a variety of applications. The ability of the antenna array to "conform" to the surface of a host platform is of great benefit primarily because of its compactness and non-obtrusiveness (reducing drag) and thus decreasing operational costs implying that, for example, airborne platforms such as fixed wing and rotary aircraft including Unmanned Aerial Vehicles (UAVs) and helicopters can maintain their designed aerodynamic characteristics while hosting an array antenna. Thus, conformal aperture arrays enable installation on airborne and space platforms as part of load bearing structure without modifying the outer mold line of the platform. They also allow wider field of view than conventional antennas and reduce size and weight requirements. The conformal antenna arrays have great potential to be utilized in systems for radar, electronic countermeasures, electronic support measures, communications, and intelligence collection. Moreover, in recent years there were many efforts to apply conformal antennas and arrays on a surface of inflatable structures - the Goddard Space Flight Center's Spartan 207/Inflatable Antenna Experiment (IAE) in 1996, utilizing conformal reflector antenna on the surface of 14-m structure. NASA estimates that large inflatable antennas will have the following advantage over current technology (advantages increase with size): (1) lower cost by 1 to 2 orders of magnitude, (2) lower stored volume 1 to 2 orders of magnitude and (3) lower mass by factors of 2 to 8 – all this being directly applicable to conformal antennas/arrays, which is an obvious if not the only choice for the inflatable antennas [1].

While today the fabrication and operation of conformal arrays in the conventional narrow-band CW or pulsed electromagnetic systems, including the radars, is a common practice, where such arrays are being built and operated on a variety of both civilian and military airborne platforms, to our knowledge, currently no conformal arrays in a transient (an impulse) regime exist. We believe that there are two primary reasons for that:

1. Implementation of radar systems in a transient regime is a relatively new phenomenon.

2. Design, fabrication and integration of an antenna array in the transient regime involves multitude of subtle elements, and while significant progress has been made recently, there still are issues not fully understood.

This SBIR-Phase I effort addresses the design and fabrication of a prototype transient multi-element planar array operating in an impulse regime. In recent years, a significant effort to further the understanding of a periodic antenna arrays, both non-planar and planar (flat), in an impulse regime was undertaken by Pro-Tech in collaboration with the researchers at the Air Force Research Laboratory's Directed Energy Directorate. Many techniques have been suggested for the purpose of launching transient electromagnetic (EM) waves and some limited results have been incorporated in the design of various EMP simulators. One such technique involves incorporating many radiating elements into an array, where the individual biconical sources (elements) are interconnected in some series/parallel configuration [2 and 3]. Clearly, the conducting surfaces that interconnect the modular sources have a significant impact on the early-time rate of rise of the radiated far field. Baum [2] studied the characteristics of the early-time far fields from infinite planar arrays of interconnected biconical sources and related the results to the late-time (low-frequency) results for the far fields from such arrays. Baum [2] developed the general formulation for array of cells, each cell consisting of two conducting cones with common apex, leading to the mathematical expressions for an effective early-time rise and early-time polarization for the far fields. Later, the same author analyzed transient arrays and their realization in EMP simulators [4 and 5]. In this paper, the author studied non-planar and planar arrays having different radiating elements (cells), including square, hexagonal and triangular cell geometries and assessed their performance analytically, by approximating large arrays as infinite for initial considerations.

The problem of impedance characterization of an incremental length of a periodic array of flat plate wave launchers in a symmetric in-line configurations was addressed in detail by Giri [6], where the numerical solution of the Laplace equation is presented, yielding all four elements of the 2×2 characteristic impedance matrix for a given set of geometrical parameters in an arbitrary cross section of the unit cell. The numerical approach yields results that agree well with three known elements, thus enhancing the confidence in the computed values for the single unknown

element of the matrix. Clearly, a precise knowledge of the array's characteristic impedance matrix is useful in arriving at optimal shapes of launcher plates (individual radiating elements). One way of launching a fast transient pulse in the TEM mode of biconic (or monoconic) antenna array geometry is to use a distributed source. Baum and Giri [7] extend this concept to that of a distributed switch, which has the potential benefit of greatly reducing the required number of switches by reducing the required size of the distributed source. While the paper addresses the case of pulsers intended to drive biconic (or monoconic) antenna arrays, the concept can be generalized for use in other types of distributed switches.

The early-time performance of periodic transient planar arrays of flat plate conical wave launchers is analyzed and reported by Giri and Baum [8], which is essentially an extension of their earlier work involving infinite planar biconical arrays. The authors report significant improvement over the planar bicones. Similar to the development of the array factor in conventional arrays, the far field is expressed in terms of the field from a single radiating element, which itself is related to the field at a reference point in the aperture of a single element. For an ideal unit step-function, the authors define an effective rate of rise in the far field, suitable for computations. In addition, two possible geometrical configurations, the symmetric and asymmetric, are identified and quantitative estimates of the effective rates of rise for both cases are made. Finally, the authors conclude that the lengths of the conical launchers in an array should be sufficiently large to obtain the improvement over the planar biconical case, but not too large to be adversely affected by the mutual interaction effects.

Baum [9] presented the available early-time analytic results for a unit radiating cell in an impulse mode to a periodic array of wave launchers [10], where the high-frequency approximation of the multiconductor transmission line equations was used. An extension of this work by considering a special case of linear variation of the launcher impedance as a function of the length coordinate along the launcher was carried out by Giri [11], where the author also analyzed high-frequency propagation characteristics of a transient array. In addition, the author determined parametric relationships indicative of the high-frequency voltage transfer characteristics from the source to the aperture plane. The results are useful in designing launcher geometries that are optimal from purely high-frequency considerations.

Both, planar arrays [2 and 3] and non-planar arrays [5 and 7] have been considered in the past. In practice, the distributed source will have to be replaced by a discrete array of modular sources Chen et al, [12]. A thorough consideration of some possible geometries associated with unit cells in the distributed-source or distributed-switch wave launcher configurations is presented by Giri et al. [8]. The authors focused their attention on one aspect of the performance, i.e., the rise time in the far field for candidate unit cell (planar conical and non-planar) designs, where the assumption was made that all sources are driven by an ideal unit step-function.

The method of stereographic projection is used to reduce the problem of calculating the TEM field distribution on two conical plates to the problem of determining the TEM field distribution on two cylindrical plates of circular arc driven by an impulse-like signals [13], where the curved-cylindrical plate problem is solved by the method of conformal mapping. While the problem addressed two launcher plates only, the results may be extrapolated to large impulse antenna arrays.

2. Technical Approach

Analogous to the conventional phased array antennas , where electronic beam control/scanning is achieved by the proper phase distribution to each radiating element via the phase shifters, we will be using the term "timed-array" antenna for an antenna array operated in a transient/impulse regime, where beam control is achieved by a proper "true-time" delays to each radiating element for generating a "coherent" radiated wave front. Such arrays have been referred to as a distributed source or a distributed switch. Here the approach consists of synthesizing the TEM mode (planar or spherical) over some aperture surface serving as the electrical source for a cylindrical or conical transmission line. Using such technique it is possible to suppress the generation of higher order (E and H) modes up to frequencies limited not by wavelengths on the order of (or larger than) the transmission line-conductor spacing and width, but by wavelengths on the order of (or greater than) the element spacing in the array forming the distributed source [10]. Such arrays are made of interconnected radiating elements, which yield current continuity

through the array, which in turn results in the array's low-frequency performance. Thus, the transient arrays are designed to have strong mutual coupling between the radiating elements forming an integral part of its operation, at least for wavelengths on the order of or larger than the inter-element spacing.

It should be pointed out at the beginning that Pro-Tech's Phase I objective is to develop a conformal impulse "timed-array" antenna, operating in a transient regime and covering a wide frequency band spanning an approximately 200 MHz-2 GHz range. Our goal is to build and test small-scale prototype impulse arrays capable of operating only in a "receive" (passive) mode.

We considered two small-scale conformal arrays capable of operating in an impulse regime. The first array will be one-dimensional (1-D) linear array consisting of 4 radiating elements, and the second array will be two-dimensional (2-D) also consisting of 4 elements. A flat (non conformal) radiator layout for both small-scale arrays is shown in Figure 1, where each radiator has flat bi-conical shaped plates to be fed at the nodes (small dark circles).

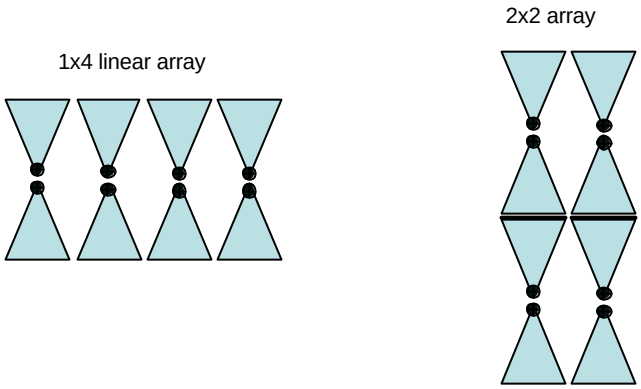

Figure 1. Radiating element layout in a 4-element 1-D and 2-D flat planar antenna arrays utilizing "bow-tie", planar bi-cones (bi-triangular shape) flat radiators.

Figure 2 presents a schematic diagram for power distribution as applied to the above 2×2 array configuration which utilizes a corporate feed in both transmit mode (left) and receive mode

(right). In the transmit mode, a voltage source $V(t)$ of impedance Z (the choice of Z can be 50Ω, 100Ω or whatever turns out to be the best for the element antenna impedance) generates a signal that reaches all four radiating elements via 4 sets of cables. The cable of impedance Z splits into 2 cables of impedance $2Z$ connected in parallel which then connects to sets of cables in series, each of which have impedance Z. Thus, there is matched impedance from the source to the antenna radiating elements.

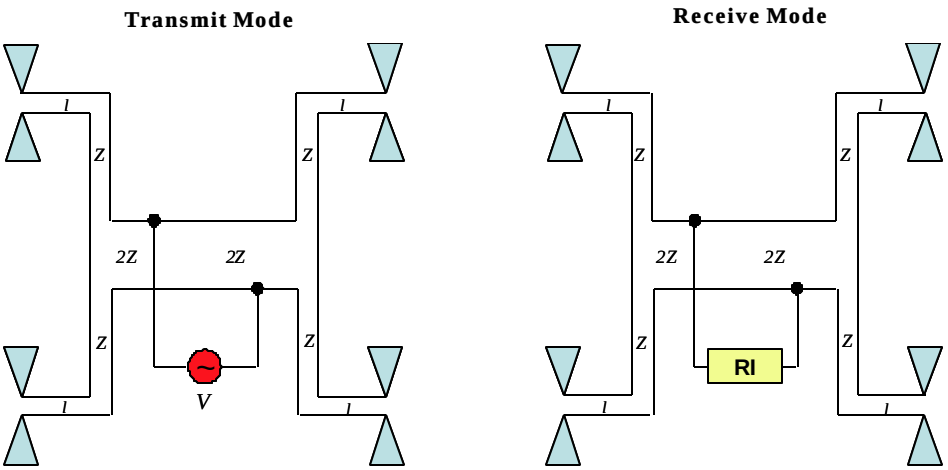

Figure 2. Schematic diagram showing power distribution in transmit and receive modes for a 2×2 array configuration using a corporate feed.

In the receive mode, the same cable of impedance 50Ω is connected to a digitizer or analog oscilloscope, labeled as Recording Instrumentation (RI). If $Z \neq 50\Omega$, then we will need the impedance matching to the scope which is typically 50 Ω. We now discuss the transition from 3-D case to 2-D case, obtained by going to the limit $l \to 0$ (see Figure 3).

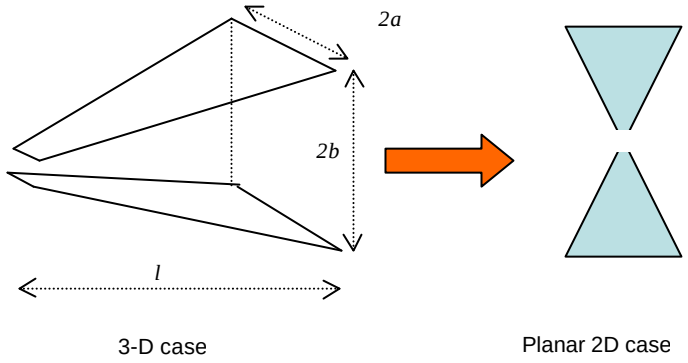

Figure 3. Transition of the radiating element from a 3-D case to a 2-D planar case.

Let us discuss briefly the impulse array's single element, consisting of a "bow-tie" or planar, flat plate bicone radiating element shown in Figure 4. ABCD is the unit cell which repeats itself in both *x*- and *y*-directions. Clearly, $\tan q = \frac{a'}{b'}$ and it follows $\frac{a'}{b'} = \frac{a}{b}$ if and only if $q = p/4$.

Table 1 presents the list of key parameters associated with the radiating element, which show the relationship between its geometrical parameters, *a, b, a', b',* q and the normalized effective rate of rise-time, $T_{n1} = ct_1/\sqrt{A}$ of the radiated field (assuming a zero rise time step function input and t_1 being the risetime of the radiated field) for planar bicones ($l/\sqrt{A} = 0$), in a symmetric configuration, for a range of realistic geometric parameters. Parameters l and $A=4ab$ represent the elementary cell depth and area respectively (see Figures 3 and 4).

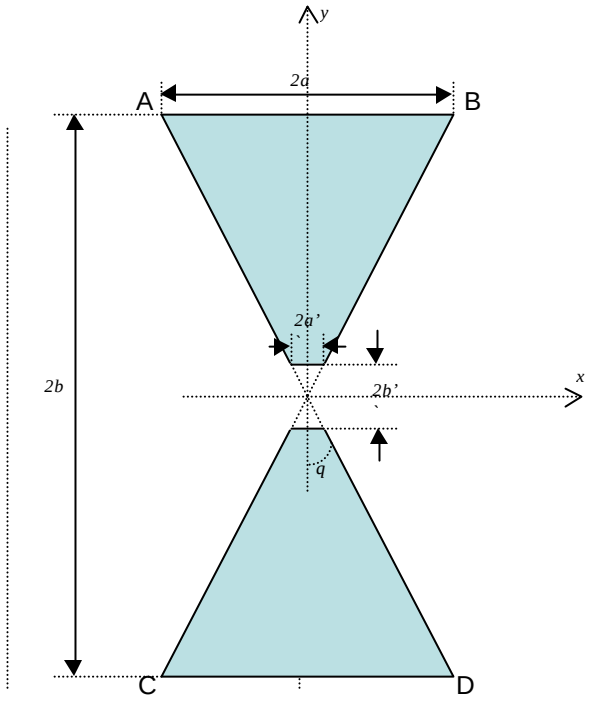

Figure 4. Details of a single radiating element configuration.

$\frac{b}{a}$	$f_{gh}(b'/a') = \frac{1}{2}\frac{b}{a}$	$\frac{2q}{p}$	q	$\frac{b'}{a'}$	$\frac{ct_1}{a}$	$T_{n1}(sym-planar) = \frac{ct_1}{\sqrt{A}}$
0.000	0.000	1.000	$0.500p$	0.000	1.000	8
0.500	0.250	0.890	$0.445p$	0.175	1.008	0.713
0.877	0.438	0.590	$0.295p$	0.751	1.115	0.595
1.000	0.500	0.500	$0.250p$	1.000	1.180	0.590
1.500	0.750	0.235	$0.118p$	2.585	1.562	0.638
2.000	1.000	0.110	$0.055p$	5.730	2.014	0.712
3.520	1.760	0.010	$0.005p$	63.657	3.527	0.940

Table 1. Normalized effective rate of rise for planar bicones ($l/\sqrt{A}$ =0), in a symmetric

configuration.

2.1 Illustrative example

Assuming *b/a = 2b/2a* =1, and consequently *b'/a' = 2b'/2a'* = 1 which yields $\theta = 0.25\pi = 45^{o}$ (see Table 1). It follows from the same table that

$$ct_1 / \sqrt{A} = 0.59$$

which yields

$$t_1 = \frac{0.59 \times \sqrt{A}}{c} = \frac{0.59 \times \sqrt{4ab}}{c}$$

In the case of 2×2 array, and *a* = *b* = 5 cm we have (see Table 1) $ct_1 / a = 1.18$ and $ct_1 / \sqrt{A} = 0.59$ yielding the same value for parameter t_1:

$$t_1 = \frac{1.18a}{c} = \frac{1.18 \times 5cm}{3 \times 10^{10} cm/\sec} \sim 200\ ps$$
$$t_1 = \frac{0.59\sqrt{4ab}}{c} = \frac{0.59\sqrt{4 \times 5cm \times 5cm}}{3 \times 10^{10} cm/\sec} \sim 200\ ps$$

Thus, if we excite the radiating element with a zero-rise time step function, we'll get a radiated pulse that has a rise time of 200 ps. Figure 5 shows the notional graphs of the input step function and the waveform of the resulting radiated field.

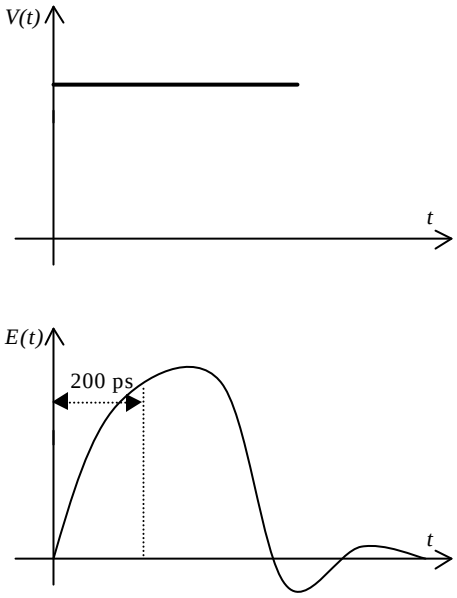

Figure 5. Input voltage (top) and the resulting radiated field (bottom).

Since the relationship between the rise time and the bandwidth is

$$\Delta f = \frac{0.35}{t_1},$$

it follows that 200 ps rise time corresponds to Δf = 1.75 GHz bandwidth! This is close to the upper bound of 200 MHz – 2 GHz range for antenna bandwidth requirements specified in the current SBIR solicitation.

As to the low-frequency end of the bandwidth, for the same 2x2 array, whose overall dimensions correspond to $4a \times 4b$ = 20cm×20cm, with the characteristic dimension being the diagonal l_c.

$$l_c = 4a\sqrt{2} = 20cm \times 1.41 \sim 28.2cm.$$

Since the antenna stops radiating and receiving when antenna characteristic dimension becomes l /2 (half of the wavelength), it follows that this low-frequency threshold can be obtained from

the following relationships:

$$\frac{l}{2} = l_c$$

which in turn yields l ~ 60 cm corresponding to approximately 500 MHz - also close to the lower bound of 200 MHz – 2 GHz range for antenna bandwidth requirements specified in the current SBIR solicitation. To achieve 200 MHz we need to employ a larger array by employing more radiating elements, e.g. utilizing 3×3 array instead of 2×2 array.

Figure 6 shows a cross-section of a small section of the conformal impulse array, showing a dielectric substrate attached to a ground conducting plane. A flat biconical radiator is immersed in the substrate and is fed by a coaxial cable from the pulser. The substrate may be fastened to the ground plane using plastic screws or bonded to it. Rogers' 3001 Bonding Film, featuring a low dielectric constant and low loss tangent at microwave frequencies, is a good candidate for bonding the substrate to the fuselage and also for bonding the flat metallic radiators (e.g. copper foil) to the dielectric substrate. This will ensure minimum interference with the electrical function of bonded stripline.

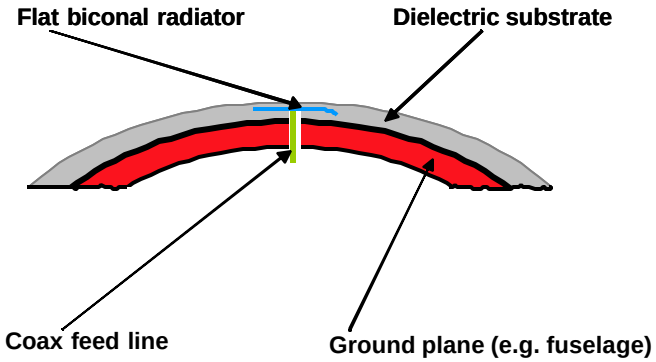

Figure 6. Cross-section of a small section (one radiating element only) of the conformal impulse prototype array utilizing flat biconical radiators.

Since the array of radiators (launchers) will be imbedded into a dielectric substrate, the choice of

substrate material is important. Large relative dielectric constant will imply larger coupling to the surface waves and thus less efficiency since part of radiation is trapped. On the other hand, thicker dielectric substrate (or larger) can support wider operational bandwidths due to "looser" electric field's fringe structure between the radiators and the ground plane (in this case the ground plane will be part of conducting cylindrical surface to which the array will be "conformed"). Table 2 presents a few candidate dielectric materials along with their characteristics, including the relative dielectric constant, dissipation factor (loss tangent) and tensile strength, all manufactured by Rogers Corporation.

Material/Character.	**RO4003C**	**RO4350B**	**Duroid 5870**	**Duroid 6002**	**Duroid 6006**	**RO4232**
Dielectric constant	3.38±0.05	3.48±0.05	2.33±0.02	2.94±0.04	6.15±0.15	3.2±0.05
Diss. Factor, tanδ	0.0027	0.0037	0.0005	0.0012	0.0027	0.0018
Tensile Modulus	3900 kpsi	1600 kpsi	189 kpsi	120 kpsi	382 kpsi	Not Avail.

Table 2. A sample of candidate substrate dielectrics and their characteristics.

The substrate properties (dielectric constant and thickness) will affect the frequency performance of the array. These effects can be seen in the expressions for the open-circuit voltage and the short circuit currents in Section 3. These effects will be quantified in numerical analyses to be carried out.

2.2 Choices made for the study

In the technical approach presented in the previous subsection, we had considered two types of arrays (linear and 2-D). After consultation with AFRL personnel, we made the following choices for study in this Phase I effort.

- Analyze, design and fabricate a 2 x 2 array as a proof of concept
- Procure Rogers Corporation material for a substrate
- Experiment with the 2 x 2 array, with a simple planar dielectric substrate

The above listed items have been completed and we present the results in the following sections.

The analysis of an array of flat-plate biconical antennas is presented in Section 3 and the experimental results are presented in Section 4.

3. Receiving Characteristics of an Ultrawideband Antenna Array

3.1 Introduction

In this note we present results obtained to date in our study of the receiving characteristics of an ultrawideband antenna array. The array comprises a number of electrically connected antennas lying in the plane $z = 0$, the interface between free space and a dielectric substrate. The substrate is of thickness d and relative permittivity ε_r, and is backed by a perfectly conducting plane at $z = -d$. The array is illuminated from the free-space region by a plane electromagnetic wave of arbitrary polarization and incidence angle. The object of the analysis is to determine the open-circuit voltages and the short-circuit currents at the antenna terminals. We work in the frequency domain, assuming and suppressing the time dependence exp (jwt) for all field quantities.

The geometry of the problem is shown in Figures 7 and 8. Figure 7 illustrates the perfectly conducting backplane at $z = -d$, the dielectric layer between $z = -d$ and $z = 0$, the perfectly conducting antenna pattern at $z = 0$, and the incident-field direction along with a rectangular coordinate system. Figure 8 shows a side view of a single antenna element centered at $(x, y) = (0,0)$. The plan view of a single antenna element is the same as in Figure 4. This element occupies a portion of the region $|x| \le a/2$, $|y| = b/2$. The terminal pair is centered at the origin and has a separation $h = 2b'$ in Figure 4 and width $w = 2a'$ in Figure 4. It is evident that $(h/w) = (b'/a') = (b/a)$, so that if the angle ϕ_a is equal to 45°, then $h/w = 1$. The feed points of other antennas in the array are located at $(x_m, y_n) = (ma, nb)$ for $m_1 < m < m_2$ and $n_1 < n < n_2$, so that the elements in the array are electrically connected.

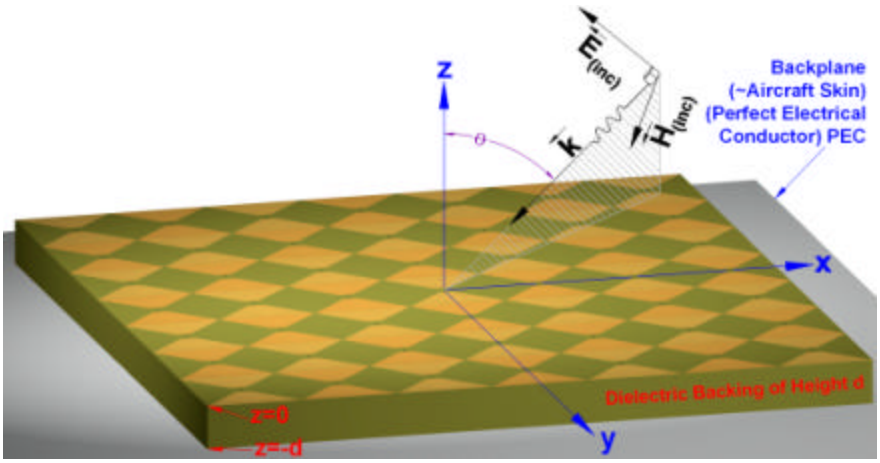

Figure 7. Geometry of the problem showing the incident plane wave on the antenna array.

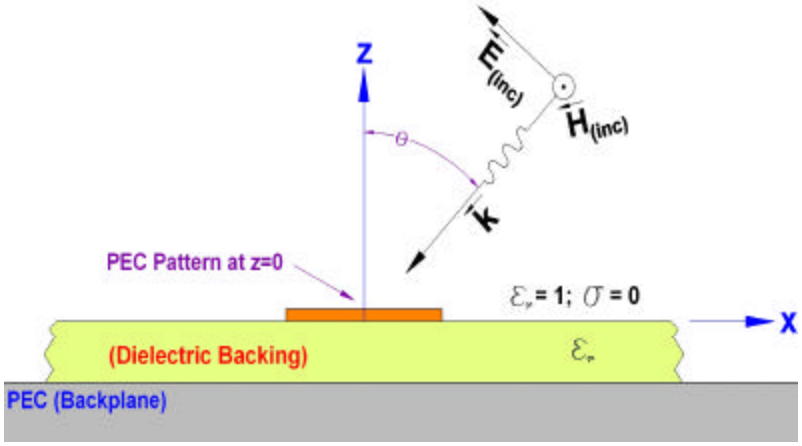

Figure 8. The central element (side view).

3. 2 Formulation of the Problem

The electromagnetic field components are derived from two scalar functions that satisfy the Helmholtz equation. We have

$$\vec{E} = -\nabla\times\Phi\vec{a}_z + \frac{Z_0}{jk_0[e_r]}\nabla\times\nabla\times\Psi\vec{a}_z \qquad (1)$$

$$\vec{H} = \nabla\times\Psi\vec{a}_z + \frac{1}{jk_0Z_0}\nabla\times\nabla\times\Phi\vec{a}_z \qquad (2)$$

in which k_0 is the wavenumber and Z_0 is the intrinsic impedance of free space, $[\varepsilon_r] = 1$ in the free-space region and $[\varepsilon_r] = \varepsilon_r$ in the dielectric layer, and the functions Φ and Ψ are solutions to the scalar Helmholtz equation.

$$(\nabla^2 + k_0^2[e_r])\begin{bmatrix}\Phi\\ \Psi\end{bmatrix} = 0 \qquad (3)$$

We write the functions Φ and Ψ in terms of Fourier integrals over the tangential coordinates as follows:

$$\begin{bmatrix}\Phi(x,y,z)\\ \Psi(x,y,z)\end{bmatrix} = \frac{1}{(2p)^2}\int_{-\infty}^{\infty}\int_{-\infty}^{\infty}\begin{bmatrix}\tilde{\Phi}(k_x,k_y;z)\\ \tilde{\Psi}(k_x,k_y;z)\end{bmatrix}e^{-jk_x x - jk_y y}dk_x dk_y \qquad (4).$$

In the free-space region, we have

$$\tilde{\Psi}_>(k_x,k_y;z) = \tilde{\Psi}_i(k_x,k_y)\,e^{jk_{z0}z} + A(k_x,k_y)\,e^{-jk_{z0}z} \qquad (5)$$

$$\tilde{\Phi}_>(k_x,k_y;z) = \tilde{\Phi}_i(k_x,k_y)\,e^{jk_{z0}z} + B(k_x,k_y)\,e^{-jk_{z0}z} \qquad (6)$$

in which $k_{z0}^2 = k_0^2 - k_x^2 - k_y^2$, $\tilde{\Psi}_i(k_x,k_y)$ and $\tilde{\Phi}_i(k_x,k_y)$ describe the incident field, and the radiation condition at $z = \infty$ is satisfied. The functions $A(k_x,k_y)$ and $B(k_x,k_y)$ are to be determined. In the dielectric layer, we have

$$\tilde{\Psi}_<(k_x,k_y;z) = -\frac{jk_{z0}e_r \cos k_{zd}(z+d)}{k_{zd}\sin k_{zd}d}\left[\tilde{\Psi}_i(k_x,k_y) - A(k_x,k_y)\right] \quad (7)$$

$$\tilde{\Phi}_<(k_x,k_y;z) = -\frac{\sin k_{zd}(z+d)}{\sin k_{zd}d}\left[\tilde{\Phi}_i(k_x,k_y) - B(k_x,k_y)\right] \quad (8)$$

in which $k_{zd}^2 = k_0^2 e_r - k_x^2 - k_y^2$. These representations for $\Phi_<$ and $\Psi_<$ make the tangential components of the electric field vanish on the conducting plane at z = -d and ensure continuity of the tangential electric field across the air-dielectric interface at $z = 0$.

For plane-wave illumination, the case of primary interest for the receiving problem and the incident-field functions $\tilde{\Psi}_i(k_x,k_y)$ and $\tilde{\Phi}_i(k_x,k_y)$ are given by

$$\tilde{\Psi}_i(k_x,k_y) = -(2p)^2 \frac{E_{0\|}}{jk_0 Z_0 \sin q}\, d(k_x - k_{xi})\, d(k_y - k_{yi}) \quad (9)$$

$$\tilde{\Phi}_i(k_x,k_y) = -(2p)^2 \frac{E_{0\perp}}{jk_0 \sin q} d(k_x - k_{xi})\, d(k_y - k_{yi}) \quad (10)$$

in which θ and ϕ are the angles of incidence in spherical coordinates, $E_{0\perp}$ is the amplitude of the incident perpendicular-polarized electric field, $E_{0\|}$ is the amplitude of the incident parallel-polarized electric field, $k_{xi} = k_0 \sin q \cos f$, and $k_{yi} = k_0 \sin q \sin f$. We express the surface current density in the plane z = 0 as the Fourier integral

$$\vec{J}_x(x,y) = \frac{1}{(2p)^2}\int_{-\infty}^{\infty}\int_{-\infty}^{\infty} \tilde{\vec{J}}_x(k_x,k_y)\, e^{-jk_x x - jk_y y} dk_x dk_y \quad (11)$$

and write $A(k_x,k_y)$ and $B(k_x,k_y)$ in terms of the incident field functions and the components of the transformed surface current density as

$$A(k_x,k_y) = -\tilde{\Psi}_i(k_x,k_y)\frac{1+P(k_x,k_y)}{1-P(k_x,k_y)} + \frac{jk_x \tilde{J}_{sx}(k_x,k_y) + jk_y \tilde{J}_{sy}(k_x,k_y)}{(k_x^2+k_y^2)\left[1-P(k_x,k_y)\right]} \quad (12)$$

$$B(k_x,k_y) = \tilde{\Phi}_i(k_x,k_y)\frac{1+Q(k_x,k_y)}{1-Q(k_x,k_y)} + \frac{k_0 Z_0}{k_{z0}}\frac{jk_y \tilde{J}_{sx}(k_x,k_y) - jkx\tilde{J}_{sy}(k_x,k_y)}{(k_x^2+k_y^2)\left[1-Q(k_x,k_y)\right]} \quad (13)$$

in which

$$P(k_x,k_y)=\frac{jk_{z0}e_r}{k_{zd}}\cot k_{zd}d \qquad (14)$$

and

$$Q(k_x,k_y)=\frac{jk_{zd}}{k_{zd}}\cot k_{zd}d \qquad (15).$$

These representations for $A(k_x,k_y)$ and $B(k_x,k_y)$ make the tangential components of the magnetic field discontinuous in the plane $z = 0$ by the amount of the (as yet unknown) surface current density $\tilde{J}_s(x,y)$.

The remaining boundary condition to be imposed is that the tangential electric field must vanish on the conducting surfaces of the antennas in the plane $z = 0$. Imposition of this condition will permit the unknown current density components $\tilde{J}_{sx}$ and $\tilde{J}_{sy}$ to be evaluated, and the solution to the problem will be complete.

3.3 Reduction to an Integral Equation

We next develop representations for the tangential electric field components in the plane $z = 0$. It is straightforward to show using eqs. (1), (4)–(6), and (12) and (13) that the transformed electric field components are expressed in terms of the transformed surface current density components by

$$\tilde{\vec{E}}_t(\vec{k}_t)=\tilde{\vec{E}}_{t0}(\vec{k}_t)-\mathbf{Z}_s(\vec{k}_t)\cdot\tilde{\vec{J}}_s(\vec{k}_t) \qquad (16)$$

with $\vec{k}_t=[k_x \;\; k_y]^T$. The impedance matrix $Z_s(\vec{k}_t)$ and the incident-field contribution $\tilde{\vec{E}}_{to}(\vec{k}_t)$ are given by

$$\mathbf{Z}_s(\vec{k}_t) = \frac{Z_0}{k_0 k_{z0}[1-Q(\vec{k}_t)]} \begin{bmatrix} k_0^2 \mathbf{I}_t - \dfrac{e_r - P(\vec{k}_t)}{e_r[1-P(\vec{k}_t)]} \vec{k}_t \vec{k}_t \end{bmatrix} \tag{17}$$

$$\tilde{\vec{E}}_{to}(\vec{k}_t) = -2j \begin{bmatrix} k_x & -k_y \\ k_y & k_x \end{bmatrix} \cdot \begin{bmatrix} Z_0 k_{z0} \tilde{\Psi}_i / [k_o (1-P)] \\ \tilde{\Phi}_i / (1-P) \end{bmatrix} \tag{18}$$

where $\mathbf{I}_t$ denotes the two-dimensional identity.

For plane-wave illumination of the array, we have from eqs. (9) and (10)

$$\tilde{\vec{E}}_{to}(\vec{k}_t) = -(2p)^2 \begin{bmatrix} \cos f & -\sin f \\ \sin f & \cos f \end{bmatrix} \cdot \begin{bmatrix} 2E_{0\|} \cos q / (1-P_i) \\ 2E_{0\perp} \cos q / (1-Q_i) \end{bmatrix} d(\vec{k}_t - \vec{k}_{ti}) \tag{19}$$

where $\vec{k}_{ti} = [k_{xi} \;\; k_{yi}]^T$ and $P_i = P(\vec{k}_{ti})$, $Q_i = Q(\vec{k}_{ti})$. Thus in the spatial domain, the incident electric field is given at $z = 0$ by

$$\tilde{\vec{E}}_{to}(\vec{x}) = \begin{bmatrix} \cos f & -\sin f \\ \sin f & \cos f \end{bmatrix} \cdot \begin{bmatrix} 2E_{0\|} \cos q / (1-P_i) \\ 2E_{0\perp} / (1-Q_i) \end{bmatrix} e^{-j \vec{k}_{ti} \cdot \vec{x}} \tag{20}$$

where $x = [x \quad y]^T$.

Enforcing the condition that the tangential electric field vanishes on the antenna surface (which is assumed to be a perfect conductor) and noting that the surface current density vanishes on those parts of the surface $z = 0$ that are not on the antennas, we obtain a pair of dual integral equations from which the surface current density, and thus the electromagnetic field, can be obtained. The first condition is expressed, using eq. (16), as

$$\frac{1}{(2p)^2} \int_{-\infty}^{\infty} \int_{-\infty}^{\infty} \mathbf{Z}_s(\vec{k}_t) \cdot \tilde{\vec{J}}_s(\vec{k}_t) e^{-j \vec{k}_{ti} \cdot \vec{x}} d^2 \vec{k}_t =$$

$$\frac{1}{(2p)^2} \int_{-\infty}^{\infty} \int_{-\infty}^{\infty} \tilde{\vec{E}}_{t0}(\vec{k}_t) e^{-j \vec{k}_i \cdot \vec{x}} d^2 \vec{k}_t \quad (\vec{x} \in S_c) \tag{21}$$

in which S_c denotes the part(s) of the surface $z = 0$ occupied by the antenna array. The fact that the surface current density vanishes off the antennas is simply expressed by eq. (22).

$$\frac{1}{(2p)^2}\int_{-\infty}^{\infty}\int_{-\infty}^{\infty}\tilde{\vec{J}}_s(\vec{k}_t)\, e^{-j\vec{k}_t\cdot\vec{x}}\, d^2\vec{k}_t = 0 \qquad (S_c \in \vec{x}) \qquad (22)$$

This pair of equations can in principle be solved for the unknown surface current density components in terms of the incident electromagnetic field.[1] The open-circuit voltages and short-circuit currents can then be evaluated.

We now convert the dual integral equations in the spatial-frequency domain into a single integral equation in the spatial domain. Since the second of the dual integral equations is simply a statement of the fact that $\vec{J}_s(\vec{x}) = 0$ for $(S_c \in \vec{x})$, we have

$$\tilde{\vec{J}}_s(\vec{k}_t) = \int\int_{S_c} \vec{J}_s(\vec{x}')\, e^{j\vec{k}_t\cdot\vec{x}'}\, d^2\vec{x}' \qquad (23)$$

where the integration domain is the surface S_c occupied by the antenna array. We substitute this expression into the first of the dual integral equations and define the scalar Green's functions $G_0(\vec{x})$ and $G_1(\vec{x})$ as

$$G_1(\vec{x}) = jk_0Z_0\frac{1}{(2p)^2}\int_{-\infty}^{\infty}\int_{-\infty}^{\infty} e^{-j\vec{k}_t\cdot\vec{x}}\,\frac{d^2\vec{k}_t}{jk_{z0}[1-Q(\vec{k}_t)]} \qquad (24)$$

and

[1] Actually, the system must be solved twice: once for the geometry in which the antenna terminal pairs are shorted together, to obtain the short-circuit currents; and once for the geometry in which the terminals are left open, to obtain the open-circuit voltages.

$$G_1(\vec{x}) = jk_0 Z_0 \frac{1}{(2p)^2} \int_{-\infty}^{\infty} \int_{-\infty}^{\infty} e^{-j\vec{k}_t \vec{x}} \frac{[e_r - P(\vec{k}_t)] d^2 \vec{k}_t}{jk_{z0} e_r [1 - P(\vec{k}_t)][1 - Q(\vec{k}_t)]} \qquad (25).$$

The first of the dual integral equations then becomes the integro-differential equation

$$\int \int_{S_c} G_0(\vec{x} - \vec{x}') J_x(\vec{x}') d^2 \vec{x}' + \frac{1}{k_0^2} \nabla_t \nabla_t \cdot \int \int_{S_c} G_0(\vec{x} - \vec{x}') J_x(\vec{x}') d^2 \vec{x}' = \vec{E}_{t0}(\vec{x}) \qquad (\vec{x} \in S_c) \qquad (26)$$

in which

$$\nabla_t = \vec{a}_x \frac{\partial}{\partial x} + \vec{a}_y \frac{\partial}{\partial y} \qquad (27)$$

is the del operator in the transverse coordinates.

Equation (26) is a form of the electric-field integral equation (EFIE). Solving it for the surface current density on the antenna array in its short-circuit configuration yields the short-circuit current at the selected antenna terminal pair. Solving it for the surface current density in the open-circuit configuration and then evaluating the tangential electric field via

$$E_t(\vec{x}) = E_{t0}(\vec{x}) - \int \int_{S_c} G_0(\vec{x} - \vec{x}') \vec{J}_s(\vec{x}') d^2 - \frac{1}{k_0^2} \nabla_t \nabla_t \cdot \int \int_{S_c} G_1(\vec{x} - \vec{x}') J_s(\vec{x}') d^2 \vec{x}' \qquad (28)$$

yields the open-circuit voltage across the selected antenna terminal pair, and the solution to our

problem is complete.

We remark that the Green's functions $G_0(\vec{x})$ and $G_1(\vec{x})$ simplify considerably if the thickness of the dielectric layer becomes large, permitting one to ignore the effects of reflections from the conducting backplane. We have as $d \to \infty$

$$G_0(\vec{x}) \to jk_0 Z_0 \frac{1}{(2p)^2} \int_{-\infty}^{\infty} \int_{-\infty}^{\infty} e^{-j\vec{k}_t \vec{x}} \frac{d^2 \vec{k}_t}{j(k_{z0} + k_{zd})} \qquad (29)$$

and

$$G_1(\vec{x}) \to jk_0 Z_0 \frac{1}{(2p)^2} \int_{-\infty}^{\infty} \int_{-\infty}^{\infty} e^{-j\vec{k}_t \vec{x}} \frac{d^2 \vec{k}_t}{j(k_{z0} e_r + k_{zd})} \qquad (30).$$

If in addition the dielectric is absent i.e., if the antenna array is situated in free space without a backing conductor, we recover the familiar result

$$G_0(\vec{x}) = G_1(\vec{x}) = \frac{jk_0 Z_0}{4p\,|\vec{x}|} e^{jk_0|\vec{x}|} \qquad (31).$$

We next investigate the possibility of obtaining approximate solutions for the short-circuit current and the open-circuit voltage.

3.4 Approximate Solutions for Terminal Current and Voltage

To develop an approximate expression for the short-circuit current at a given terminal pair we invoke the physical-optics (PO) assumption that the surface current density on the antennas is equal to $\vec{J}_s = 2\vec{a}_z \times \vec{H}_i$, with $\vec{H}_i$ denoting the incident magnetic field. It is easily shown that for plane-wave illumination, the PO surface current density components are given for $(x, y) \in S_c$ by

$$J_{sx}^{PO}(\vec{x}) = \frac{2}{Z_0}(E_{0\|}\cos f - E_{0\perp}\cos q \sin f)\, e^{-j\vec{k}_{ti}\cdot\vec{x}} \qquad (32)$$

$$J_{sx}^{PO}(\vec{x}) = \frac{2}{Z_0}(E_{0\|}\sin f - E_{0\perp}\cos q \cos f)\, e^{-j\vec{k}_{ti}\cdot\vec{x}} \qquad (33)$$

We assume that the antennas in the array are disposed so that the short-circuit current flows in the *y* direction and the electric field across open terminal pairs is also oriented in the *y*-direction. The short-circuit current across the terminal pair at $(x, y) = (x_m, y_n)$ is simply

$$I_{sc,mn} = \frac{2}{Z_0}(E_{0\|}\sin f - E_{0\perp}\cos q \cos f)\, e^{-j\vec{k}_{ti}\cdot\vec{x}_{mn}} \qquad (34)$$

where w is the width of the shorting connector. It is assumed that w is small compared to the shortest wavelength of interest. In the special case for which the illuminating plane wave is normally incident on the antenna and is polarized in the *y*-direction, the above result simplifies to

$$I_{sc} = \frac{2E_{0\perp}w}{Z_0} \qquad (35)$$

The open-circuit voltage across the terminal pair that is centered at (x_m, y_n) and that has a gap width *h* is expressed in terms of the surface current density $\vec{J}_s(\vec{x})$ as

$$V_{oc,mn} = E_{t0y}(\vec{x}_{mn})\, h - \int_{y_n - h/2}^{y_n + h/2} dy \int\int_{S_c} G_0(x_m - x', y - y')\, J_{sy}(\vec{x}')\, d^2\vec{x}' - \frac{1}{k_0^2}\left[\nabla_t \cdot \int\int_{S_c} G_1(\vec{x} - \vec{x}')\, \vec{J}_s(\vec{x}')\, d^2\vec{x}'\right]_{x=x_m, y=y_n - h/2}^{x=x_m, y=y_n + h/2} \qquad (36)$$

The gap width h is assumed to be small in comparison to the shortest wavelength of interest.

We shall attempt to evaluate this expression using the PO surface current density, setting $\vec{J}_x(\vec{x}') = \vec{J}_x^{PO}(\vec{x}')$. In the special case for which the illumination of the array is a *y*-

polarized, normally incident plane wave, we obtain

$$V_{oc,mn} = \frac{2E_{0\perp}h}{1-Q_\perp} - \frac{2E_{0\perp}}{Z_0}\int_{y_n-h/2}^{y_n+h/2} dy \int\int_{S_c} G_0(x_m - x', y - y')\, d^2\vec{x}' - \frac{2E_{0\perp}}{Z_0}\frac{1}{k_0^2}\left[\frac{\partial}{\partial y}\int\int_{S_c} G_1(x_m - x', y - y')\, d^2\vec{x}'\right]_{y=y_n-h/2}^{y=y_n+h/2} \qquad (37)$$

with

$$Q_\perp = j\sqrt{e_r}\cot(k_0 e_r d) \qquad (38).$$

Denoting by $\tilde{S}_c(k_x, k_y)$, the Fourier transform of the conducting pattern of the antennas on the surface $x = 0$ and shifting coordinates so that the antenna terminal pair is located at $(x, y) = (0, 0)$, we find that the above expression can be written in the form

$$\frac{V_{oc,mn}}{E_{0\perp}h} = \frac{2}{1-Q_\perp} - \frac{2}{Z_0}\frac{1}{(2p)^2}\int_{-\infty}^{\infty}\int_{-\infty}^{\infty}\tilde{G}_0(k_x, k_y)\,\tilde{S}_c(k_x, k_y)\,\mathrm{sinc}(k_y h/2)\,dk_x dk_y + \frac{2}{k_0^2 Z_0}\frac{1}{(2p)^2}\int_{-\infty}^{\infty}\int_{-\infty}^{\infty}\tilde{G}_1(k_x, k_y)\,\tilde{S}_c(k_x, k_y)\,\mathrm{sinc}(k_y h/2)\,k_y^2\,dk_x dk_y \qquad (39)$$

We evaluate the transformed antenna geometry $\tilde{S}_c(k_x, k_y)$ for a two-dimensional rectangular array of "butterfly" antennas. Let the feed points of the individual antennas be located at $(x_m, y_n) = (ma, nb)$ for $m_1 \le m \le m_2$ and $n_1 \le n \le n_2$. Then

$$\tilde{S}_c(k_x, k_y) = \tilde{S}_0(k_x, k_y)\sum_{m=m_1}^{m_2}\sum_{n=n_1}^{n_2} e^{jk_x x_m + jk_y x_n} \qquad (40)$$

in which $\tilde{S}_0(k_x, k_y)$ is the transform of a single antenna element. For the 45° butterfly antennas under consideration here, it is easy to show that

$$\tilde{S}_0(k_x,k_y)=\frac{2}{k_x}\left[\frac{\cos(k_x-k_y)h/2-\cos(k_x-k_y)a/2}{k_x-k_y}+\right.$$
$$\left.\frac{\cos(k_x-k_y)h/2-\cos(k_x-k_y)a/2}{k_x+k_y}\right] \qquad (41).$$

Now it is not difficult to show that the second of the integrals in eq. (39) above does not exist. This is a consequence of our use of the PO currents which do not satisfy the proper edge conditions. The result is an infinitely large imaginary component of the open-circuit voltage, and thus of the equivalent impedance at the antenna terminals. However, if we simply ignore this component and also assume that the signal frequency is very large, the integral contributions to the open-circuit voltage become negligible and the open-circuit voltage is simply

$$V_{oc,mn}=\frac{2E_{0\perp}h}{1-Q_\perp} \qquad (42).$$

The result will be valid at high frequencies or early times.

3.5 Equivalent Source Impedance

The ratio of the open-circuit voltage to the short-circuit current is the high-frequency Thèvenin impedance Z_T, given by

$$\frac{Z_T}{Z_0}=\frac{\tan f_a}{1-j\sqrt{e_r}\cot(k_0\sqrt{e_r}d)}=\frac{\tan f_a}{\sqrt{e_r}+1}(1-e^{-2jk_0\sqrt{e_r}d})\sum_{n=0}^{\infty}R^n e^{-2jnk_0\sqrt{e_r}d} \qquad (43)$$

in which we have written $h/w=\tan f_a$ and R denotes the internal reflection coefficient at the air-dielectric interface.

$$R=\frac{1-\sqrt{e_r}}{1+\sqrt{e_r}} \qquad (44)$$

Note that if the relative permittivity of the dielectric layer is equal to unity, then $R = 0$ and

$$\frac{Z_T}{Z_0} = \frac{1}{2}\tan f_a (1 - e^{-2jk_0\sqrt{e_r}d}) \qquad (e_r = 1) \qquad (45)$$

in which the effect of the single reflection at the conducting plane is evident. If, on the other hand, the thickness of the dielectric layer becomes large, we have

$$\frac{Z_T}{Z_0} = \frac{\tan f_a}{\sqrt{e_r} + 1} \qquad (d \to \infty) \qquad (46)$$

in which the loading effect of the dielectric layer is evident.

The results above are easily generalized to the case in which the angle of incidence and the polarization of the illuminating plane wave are arbitrary. We define the field amplitude E_0 and the polarization angle α such that

$$E_{0\perp} = E_0 \cos a \qquad E_{0||} = E_0 \sin a \qquad (47)$$

then the open-circuit voltage is [cf. eq. (20)]

$$V_{oc} = 2E_0 h \left[\frac{\sin a \cos q \sin f}{1 - P_i} + \frac{\cos a \cos f}{1 - Q_i} \right] \qquad (48)$$

with

$$P_i = \frac{j\varepsilon_r \cos\theta}{\sqrt{\varepsilon_r - \sin^2\theta}} \cot(k_0 d\sqrt{\varepsilon_r - \sin^2\theta}) \tag{49}$$

$$Q_i = \frac{j\sqrt{\varepsilon_r - \sin^2\theta}}{\cos\theta} \cot(k_0 d\sqrt{\varepsilon_r - \sin^2\theta}) \tag{50}$$

The short-circuit current is expressed [cf. eq. (34)]

$$I_{sc} = \frac{2w E_0}{Z_0}(\sin\varepsilon \sin\phi + \cos\alpha \cos\theta \cos\phi) \tag{51}$$

thus we obtain the Thèvenin impedance in the general case

$$\frac{Z_T}{Z_0} = \tan\phi_a \frac{(1-Q_i)\sin\alpha \cos\theta \sin\phi + (1-P_i)\cos\alpha \cos\phi}{(1-P_i)(1-Q_i)(\sin\alpha \sin\phi + \cos\alpha \cos\theta \cos\phi)} \tag{52}$$

It is easy to show that for near-normal incidence (i.e., to second order in a), the result above reduces to that given in eq. (43).

3.6 Concluding Remarks for the Analysis

We have formulated the problem of a receiving antenna array situated in an air-dielectric interface and backed by a perfectly conducting plane. We obtained an integro-differential equation for the surface current density on the array surface. The short-circuit currents and the open-circuit voltages can be evaluated exactly, once this equation is solved and the surface current density is known. A numerical approach will be required for this purpose.

We have also developed simple approximate expressions for the short-circuit current and the open-circuit voltage at the antenna terminals. The short-circuit current was estimated on the basis of the physical-optics approximation. The open-circuit voltage was estimated at early times (or high frequencies) from the PO currents, ignoring an infinite imaginary component that results from the fact that the PO currents do not satisfy the proper edge conditions. The ratio of

the open-circuit voltage to the short-circuit current is the equivalent Thèvenin impedance of the source that is effectively applied to the antenna terminals in the receive mode. The general expression for this quantity was given in eq. (52). At near-normal incidence, the Thèvenin impedance reduces to the expression given in eq. (43) and expressions for the impedance in the limiting cases for which $e_r \to 1$ or $d \to \infty$ are given in eqs. (45) and (46).

The next step to be taken in the analysis of this problem is to develop an exact numerical solution to the integral eq. (26) for the surface current density on the antenna array. From this solution one may then construct exact expressions for the short-circuit currents and the open-circuit voltages at the antenna terminals.

This is the present status of our analysis and we anticipate continuing this and developing numerical solutions to the formulation presented above.

In the next section, we describe the experimental design, fabrication and performance characteristics of the 2-D array.

4. Experimental Results

4.1 Introduction

During the SBIR phase-I effort, a prototype four element conformal antenna was built and evaluated. The antenna utilizes a nylon substrate to reduce costs and to avoid modification of the expensive Duroid material for future experiments. The results indicate that the theoretical basis for the antenna is correct and that some simple improvements can be done to substantially improve the performance. The antenna is driven by a single 50 Ω source. The 50 Ω source drives two 100 Ω coaxial cables connected in parallel with each 100 Ω cable driving two parallel 200 Ω strip line cables. The four strip line cables drive each of the four antenna elements. Ferrite cores are placed on the outer conductor of the 100 Ω cables to provide isolation between the individual elements of the array. The array was evaluated in the time and frequency domain. The array was then modified to improve the low frequency response and the measurements were repeated.

4.2 Fabrication of the Prototype Array

A four element (2x2) prototype conformal antenna was fabricated. The array elements measure 10 cm x 10 cm (width x height) and were formed using 0.2 mm thick copper tape placed on a 6.35 mm thick nylon plate. A top view of the array is shown in Figure 9. A Prodyn Technologies SB-10D (Serial Number 29) summing block is used to interface the two 100 Ω feed cables to the 50 Ω feed cable. The two 100 Ω feed cables interface with four 200 Ω strip transmission lines that are machined into the nylon substrate of the array. Three Ferrite cores were placed on each 100 Ω cable to provide isolation between the two arrays. The interface between the 100 Ω cable and the two 200 Ω cables is shown in Figure 10. The length of the center conductor required to connect to the 200 Ω line introduced a significant parasitic inductance that was partially compensated for by placing a small amount of epoxy (dielectric constant of 5.1) at the feed point.

4.3 Experimental Evaluation of the Prototype Array

The array was evaluated in the time domain using a TDR and in the frequency domain with a network analyzer. A Tektronix 11801A sampling oscilloscope with an SD-24 TDR head was using to make the TDR measurements of the array. A Hewlett Packard 8753 frequency domain network analyzer is used to measure S11. The SWR for the array is obtained from the S11 measurement.

The TDR measurement is shown in Figure 11. The interface between the 100 Ω and the 200 Ω transmission lines is clearly evident. Also, the end of the elements can be seen clearly. The S11 (magnitude and phase) and SWR (calculated from the S11 measurement) are shown in Figures 12, 13 and 14. The SWR drops below 1.75 at 598.8 MHz and remains below 1.75 up to 1.67 GHz.

In an attempt to extend the low frequency cutoff of the array, two extensions (“wings”) were added to the antenna elements. The wings as installed on the array are shown in Figure 15. The

dimensions of the extension are 20 cm by 14.6 cm (width x height). The TDR of the antenna with extensions is shown in Figure 16. The 100 Ω to (2x) 200 Ω interface and the interface between the 200 Ω lines and the antenna elements are similar to the previous measurements. A significant difference is noted at the end of the antenna elements. The system remains approximately matched for a much longer period of time. As is shown in Figure 17, the additional time is approximately 2.5 ns. The S11 (magnitude and phase) and SWR measurements for the modified array are shown in Figures 18, 19 and 20. The low frequency cutoff (SWR less than 1.75) is reduced to 296 MHz by adding the extensions.

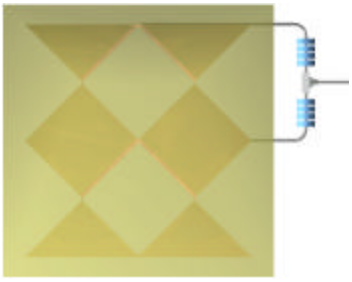

Figure 9. Antenna fabricated for Phase I experiments.

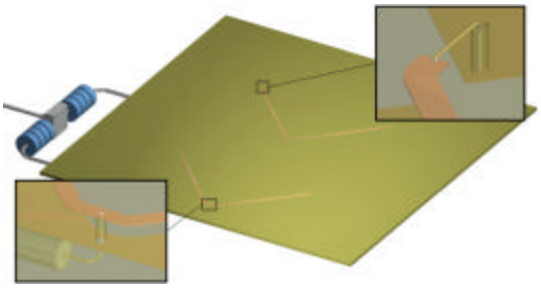

Figure 10. Coaxial 100 Ω – 200 Ω Strip transition.

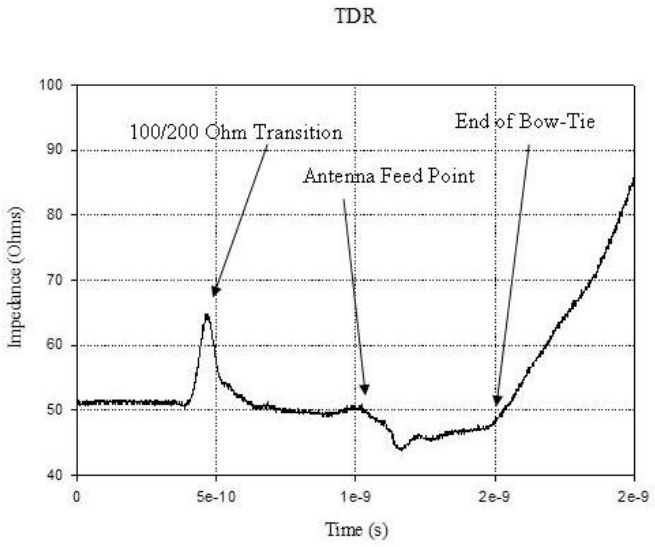

Figure 11. TDR measurement of prototype array.

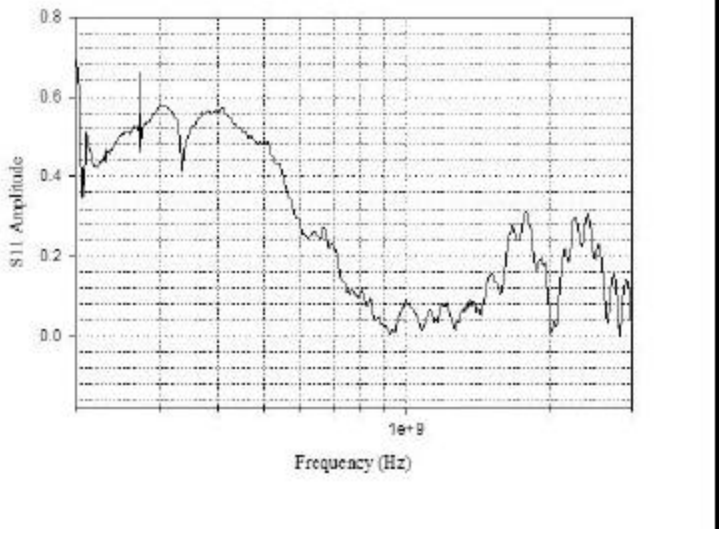

Figure 12. S11 (amplitude) measurement of prototype array.

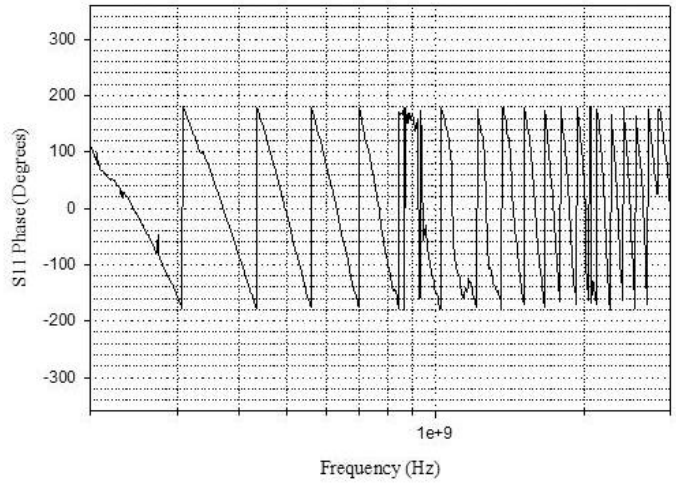

Figure 13. S11 (Phase) measurement of prototype array.

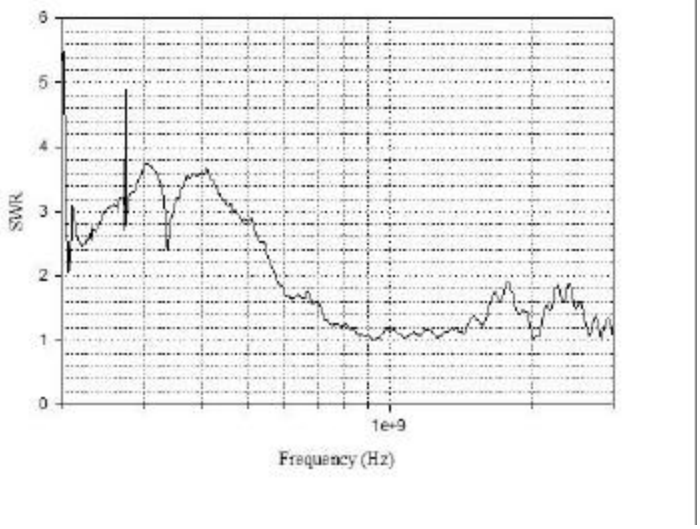

Figure 14. SWR (calculated from S11 measurement) for the prototype array.

Figure 15. Photo of the prototype array with the extensions installed.

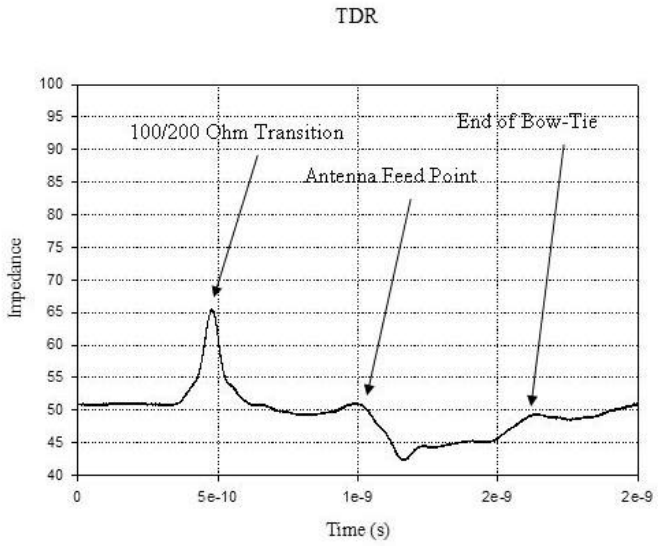

Figure 16. TDR of prototype array with the extensions.

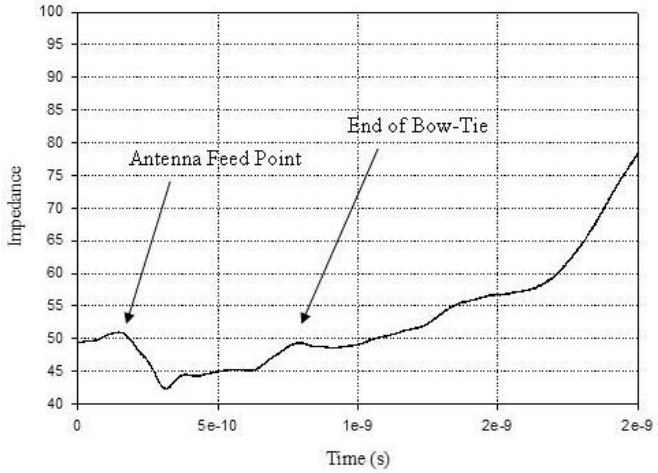

Figure 17. TDR measurement showing the end of the extensions.

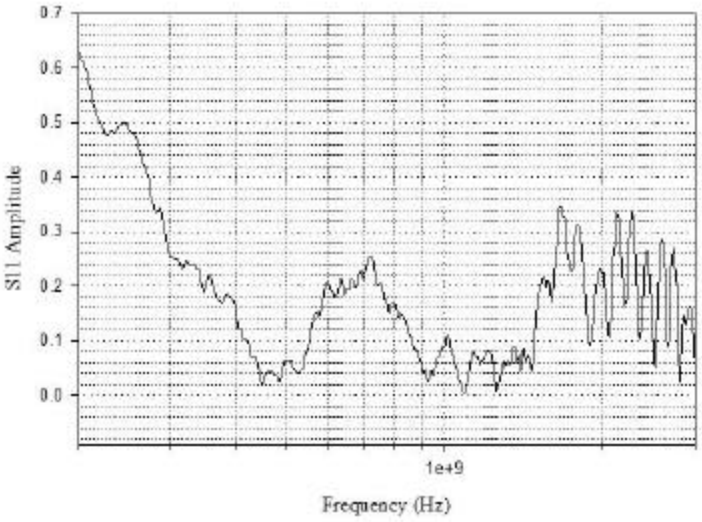

Figure 18. S11 measurement for the prototype array with the extensions.

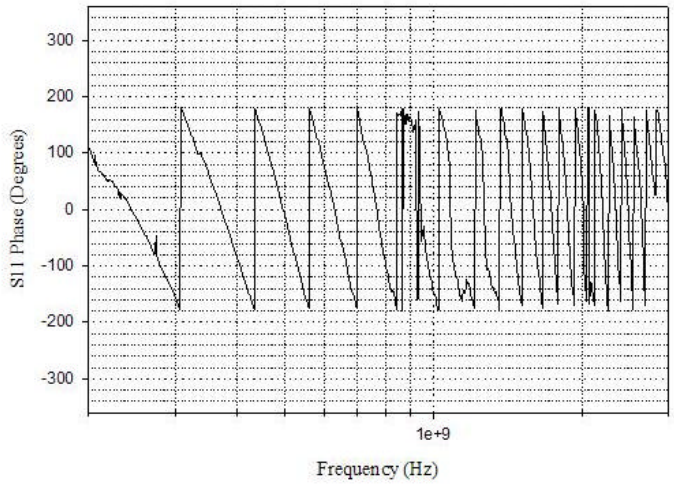

Figure 19. S11 Phase for the prototype array with the extensions.

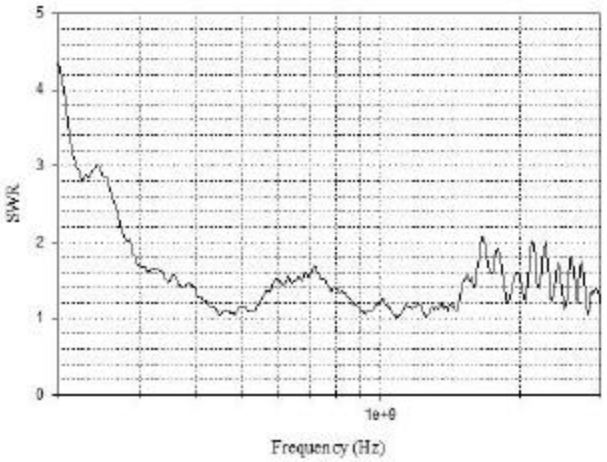

Figure 20. SWR for the prototype array with the extensions.

5. Summarizing Remarks

5.1 Analysis of the Antenna Array

Under this Phase I effort, we have formulated the receiving characteristics of a hyperband antenna array. The array consists of a number of electrically connected elements lying in the plane z = 0, the interface between free space and dielectric substrate. The substrate is of thickness d and relative permittivity e_r, and is backed by a perfectly conducting plane at z = $-d$. The array is illuminated from the free space region by a plane electromagnetic wave of arbitrary polarization and incidence angle. We are now able to determine the open-circuit voltages and the short–circuit currents at the antenna terminals. We work in the frequency domain assuming and suppressing the time dependence $exp\ (\ jwt\ )$ for all field quantities. A numerical approach will be required for the purpose of completing the analysis.

We have also developed simple approximate expressions for short-circuit current and open-circuit voltage at the antenna terminals. The short-circuit current was estimated on the basis of the physical optics approximation. The open-circuit voltage is estimated at early times (high-frequencies) from the Physical Optic currents, ignoring the infinite imaginary components that result from the fact that the Physical Optic current do not satisfy the proper edge conditions. The ratio of the open-circuit voltage to the short-circuit current is the equivalent Thevenin impedance of the source that is effectively applied to the antenna terminals in the receive mode.

Under the Phase II effort, the next step is to develop an exact numerical solution to the integral equation for the surface current density on the antenna array. From this solution, one may then construct exact expressions for the short-circuit currents and open-circuit voltages at the antenna terminals.

5.2 Proof-of Concept Experiments Performed in Phase-I

During this SBIR Phase I effort, a mock-up four element conformal antenna was built and evaluated. The antenna utilizes a nylon substrate to reduce costs and to avoid modification of the

expensive Duroid material for future experiments. The results indicate that the theoretical basis for the antenna is valid and that some simple improvements can be done to substantially improve the performance. The antenna is driven by a single 50 Ω source. The 50 Ω source drives two 100 Ω coaxial cables connected in parallel with each 100 Ω cable driving two parallel 200 Ω strip line cables. The four strip line cables drive each of the four antenna elements. Ferrite cores are placed on the outer conductor of the 100 Ω cables to prevent low frequency shorting of the antenna. In the mock-up antenna, the transition from the 100 Ω cables to the two 200 Ω cables is somewhat inductive. Some capacitive compensation is used to improve the impedance match; however, significant improvement can be realized. The antenna was not tested on a substrate similar to that of a typical application for this type of conformal array. During the Phase II effort, the four element antenna will be optimized and built on a Duroid substrate and the array will be tested with a component of a UAV. Antenna extensions will be added to improve the low frequency response of the antenna. Antenna radiation pattern measurements will be performed to determine the effects of the UAV component.

The antenna used for the Phase II experiments will be similar to what has been used in Phase I effort. The new antenna will utilize Rogers 5870 Duroid as a substrate. The dielectric constant for Duroid remains relatively constant (2.31-2.35) for frequencies up to 10 GHz. The 200 Ω transmission lines will be formed on opposite sides of the 0.125" thick material. Detailed attention will applied to the transition from the 100 Ω coaxial transmission line to the 200 Ω lines. The TDR data of the transition from the 100 Ω line into 2 x 200 Ω lines in parallel indicates that the inductance of the connection is too high. The length of this connection and the therefore the inductance will be reduced by embedding the coaxial cable in dielectric to allow shortening of the connection. Additional ferrite beads will also be added to extend the low frequency range of the spectrum.

5.3 Phase II Technical Objectives

It is anticipated that the Phase II program will progress in mainly 4 parts:

1. Complete the analyses started in Phase I by developing the numerical approaches to solve for the Thevenin equivalent circuits at antenna array elements.

2. Design a suitable array to meet the following goals; perform numerical analysis of this optimal array.

    - Develop and demonstrate design concepts for electromagnetic impulse receive antenna arrays (This has been done in Phase I)
    - Minimize the depth of the conformal array (also accomplished in Phase I)
    - Capable of being conformably mounted on the body or wing of airborne platforms
    - Frequencies of interest from approximately 200 MHz to 2.0 GHz
    - The goal for the frequency response over this range is +/- 5 dB
    - The antenna gain should be as high as feasible
    - Additionally, antennas that can be fabricated of flexible conductive materials that can be bonded to inflatable structures are highly **desirable**
    - The output from each element of the array should be capable of being interconnected so as to allow a single analog output or individually connected to waveform digitizers
3. We will fabricate a section of the structural element of a notional UAV, provide the design details, perform tests and provide electrical properties.
4. Integrate the hardware developed in (3) and the optimally designed array system for antenna performance tests.

6. Specific Tasks for Phase II

We have proposed to perform the following tasks in the Phase-II effort.

Task 1: **Numerical modeling of the antenna array**

Obtaining an exact solution for the problem of UWB signal reception and transmission by a multi-element array requires that we solve a certain integro-differential equation for the surface current density on the array. This equation must be solved by numerical means; and in this task, we will develop and explore the numerical solution. We will obtain numerical results for the short-circuit current and the open-circuit voltage at the antenna terminals on

receive, and for the radiated field on transmit.

Task 2: Analytical modeling of the array on a curved surface

The applications that are intended for the UWB antenna array might require that the array be made conformal to a curved surface. It is therefore important that the effects of curvature on the array's reception and transmission properties be understood. In this task, we will extend the analytical work already completed for the planar array, in order to examine the behavior of a similar array that is conformal to a cylindrical surface.

Task 3: Modeling in support of specific experiments

It is anticipated that some analytical and numerical modeling work will be required to support certain specific experimental configurations that will be used during Phase II. Precisely what modeling work will be required is not at present known.

Task 4: Material and Process Development and Validation

The objective of this task is to fabricate and characterize a composite back plane for the installation of a full-scale 2-D impulse antenna array made of bow tie radiators.

In order to construct an appropriate set of panels that would be useful for validating end-use properties of a broad spectrum of airframes, we'll assess some service parameters from a portfolio of Northrop Grumman military airplane platforms, ex. F/A-18, Global Hawk, etc.

After establishing Requirement Definition of a composite antenna backplane, we'll investigate and select a potential composite material candidate for the skin panel. We'll build composite skin flat panels to fabricate specimens in order to evaluate typical chemical, physical, mechanical, and electrical characteristics of a dielectric material in a variety of temperatures and

conditioning environments and designate deterministic material design values. Under this task we will fabricate a small, not full scale, conformal composite skin panel, with the potential composite material candidate on an available prototype aluminum tool for the remaining Phase II activities. [Ref: MIL-HDBK-17F, Volume 1, Polymer Matrix Composites Guidelines for Characterization of Structural Material].

Task 5. Our team will build a four element conformal array similar to that built for the Phase I effort. The Duroid (Rogers 5870) material procured during the Phase I effort will be utilized as a substrate.

Task 6. Measurements will be performed to determine S11, VSWR. TDR measurements will also be made. The antenna will then be optimized using these measurements.

Task 7. Antenna "wings" will be fabricated and installed on the antenna and the S11, VSWR and TDR measurements will be repeated.

Task 8. Antenna pattern measurements will be made in the 909 chamber using time domain techniques. Measurements will be performed with and without the wings installed.

Task 9. The antenna will be installed on a piece of UAV structural component. S11, VSWR and TDR measurements will be repeated to determine effects of the component.

Task 10. Modifications to the antenna will be performed to optimize antenna performance with the UAV component.

Task 11. Antenna pattern measurements will be made with the UAV component in the 909 chamber. Measurements will be made with and without the wings installed.

Task 12. Detailed antenna pattern and gain measurements over the bandwidth of 200 MHz to 2 GHz will be performed at Antcom Corporation, Torrance, CA. They have a capability to make these measurements in time and frequency domains. Dr. Giri will participate in these tests.

Task 13: **Documentation**

References:

[1] Caille G, Vourch E, Martin M, Mosig A Iversen P. 1998. Conformal Array Antenna for LEO Observation Platform. European Microwave Conference, 1998.

[2] Baum CE. 1973. Early Time Performance at Large Distances of Periodic Planar Arrays of Bicones with Sources Triggered in a Plane-Wave Sequence. Sensor and Simulation Note 184, 30 August 1973.

[3] Baum CE. 1970. Some Characteristics of Planar Distributed Sources for radiating Transient Pulses. Sensor and Simulation Note 100, 12 March 1970.

[4] Baum, CE. 1978. "EMP Simulators for Various Types of Nuclear EMP Environments: An Interim Categorization. Sensor and Simulation Note 240, January 1978 and Joint Special Issue on the Nuclear Electromagnetic Pulse, IEEE Transactions on Antennas and Propagation, January 1978, pp. 35-53, and IEEE Transactions on Electromagnetic Compatibility, February 1978, pp. 35-53.

[5] Baum CE. 1969. The Distributed Source for Launching Spherical Waves. Sensor and Simulation Note 84, 2 May 1969.

[6] Giri DV. 1989. Impedance Matrix Characterization of an Incremental length of a periodic Array of Wave Launchers. Sensor and Simulation Note 316, 1 April 1989.

[7] Baum CE. and Giri DV. 1985. The Distributed Switch for Launching Spherical Waves. Sensor and Simulation Note 289, 28 August 1985.Note 84.

[8] Giri DV and Baum CE. 1987. Early Time Performance at Large Distances of Periodic Arrays of Flat-Plate Conical Wave Launchers. Sensor and Simulation Note 299, 1 April 1987.

[9] Baum CE. 1989. Canonical Examples for High-Frequency Propagation on Unit cell of

Wave-Launcher Array. Sensor and Simulation Note 317, 19 April 1989.

[10] Baum CE. "Transient Arrays", pages 129-138, Ultra-Wideband, Short-Pulse Electromagnetics 3, Plenum Press, New York, 1997, ISBN 0-306-45593-5.

[11] Giri DV. 1989. A family of Canonical Examples for High Frequency Propagation on Unit cell of Wave-Launcher Array. Sensor and Simulation Note 318, 5 June 1989.

[12] Chen YG, Giri DV et al. 1986. Design Procedures for Arrays which Approximate a Distributed Source at the Air-Earth Interface. Sensor and Simulation Note 292, 1 May 1986.

[13] Yang FC and Marin L. 1977. Field Distribution on a two-Conical-Plate and a Curved Cylindrical-Plate Transmission Line. Sensor and Simulation Note 229, September 1977.

DISTRIBUTION LIST

DTIC/OCP 8725 John J. Kingman Road, Suite 0944 Ft. Belvoir, VA 22060-6218	1 cy
AFRL/VSIL Kirtland AFB, NM 87117-5776	2 cys
AFRL/VSIH Kirtland AFB, NM 87117-5776	1 cy
Official Record Copy AFRL/DEHP/Lt Joe Broeckert	2 cys

(This page is intentionally left blank)